Differentiation methods of rat brain tissues and glioma model 101.8 *ex vivo* using optical coherence tomography

© *P.V. Aleksandrova* [1,2], *K.I. Zaytsev* [1], *P.V. Nikitin* [3], *A.I. Alekseeva* [4], *A.A. Nebezhev* [5],
  V.I. Polshina [5], *P.A. Karalkin* [5], *I.N. Dolganova* [2,¶]

[1] Prokhorov Institute of General Physics, Russian Academy of Sciences,
119991 Moscow, Russia
[2] Osipyan Institute of Solid State Physics RAS,
142432 Chernogolovka, Russia
[3] University of Houston,
Houston, Texas, the USA
[4] Avtsyn Research Institute of Human Morphology of Federal State Budgetary Scientific Institution „Petrovsky National Research Centre of Surgery",
117418 Moscow, Russia
[5] Sechenov First Moscow State Medical University (Sechenov University),
119991 Moscow, Russia
e-mail: aleksandrovapolina98@gmail.com
¶ e-mail: in.dolganova@gmail.com

The article considers two methods of image analysis obtained by using optical coherence tomography (OCT): analysis of attenuation coefficient and speckle-structures of images as regards differentiation of intact tissues and rat brain tumors. The glioma model 101.8 was used for extracting information from speckle structures using wavelet analysis method of OCT images and calculating the power of local brightness fluctuations in speckles. Applying linear discriminant analysis, the effectiveness of the developed approach consisting of two methods was evaluated on the basis of sensitivity, specificity and precision values in differentiation of glioma model and intact tissues. The results of the study showed the advantages of the developed OCT image analysis method for neurosurgery.

Keywords: optical coherence tomography, glioma, wavelet analysis, Fisher linear discriminant analysis, speckle structure, attenuation coefficient.

Introduction

Optical coherence tomography is a label-free method (it uses only endogenous (i.e., internal, intrinsic to the sample itself) diagnostic markers) that allows one to establish a contrast between signals from objects with different scattering properties [1–5]. OCT has demonstrated clinical utility for the study and detection of abnormalities in various organs, including retina, coronary vessels, skin, breast, and brain [6–9]. It has shown great potential in the diagnosis and surgery of glial brain tumors [11–24], which is exemplified by its capacity to visualize melanoma metastases [10]. Glial tumors forming from the cells of white brain matter are characterized by invasive growth, which complicates their diagnosis. A number of *in vivo* and *ex vivo* studies have verified the capacity of OCT to detect tumor growth boundaries via qualitative and quantitative signal assessment [15,25–27].

Most existing OCT signal processing methods are based on intensity analysis and extraction of scattering and attenuation coefficients. According to the obtained experimental data, the attenuation coefficient for glial tumors is lower than for intact tissues (including the cortex and white matter [20,22,23]). White matter is characterized by the presence of nerve fibers covered with a myelin sheath, which is the reason why the attenuation coefficient is higher than the one corresponding to the cortex. In OCT images, the cortex appears similar to tumor tissue [24,28]. Thus, given the label-free nature of OCT, further development of OCT image processing algorithms is required in order to increase the sensitivity and specificity.

One possible method for improving neurodiagnostics with OCT is the analysis of speckle patterns that emerge in OCT images due to the interference of a large number of elementary waves with random phases that arise in propagation of coherent light through a scattering medium. Since most biological tissues are heterogeneous, speckle patterns will always appear when an object is illuminated with coherent light. They may both distort measurements and provide useful data on the structural properties of a sample [29–31]. These patterns are a source of noise in images obtained under coherent light illumination and reduce the image quality and contrast, blurring the boundaries between different tissue types. However, recent OCT

Table 1. Rat brain tissue samples

Tissue type	Number of samples	Number of B-scans
Cortex	12	31
White matter	12	28
Glioma model 101.8	9	20

imaging research [29] has demonstrated that speckles may contain data on the structural properties of examined tissues. A statistical study was carried out in [32], and it was shown that the boundary of skin layers may be determined from the distribution of speckle patterns in OCT images. The same research technique was applied in [33] to the corneas of the eye. Thus, assuming that speckle patterns are related to the properties of the tissue under study, their analysis may be used for brain tissue differentiation in OCT images.

OCT images of intact tissues and rat glioma model 101.8 were obtained and examined for the purpose of brain tissue differentiation. In the present study, the power of local brightness fluctuations in a speckle and its standard deviation were calculated via wavelet analysis of OCT images. The attenuation coefficient and its dispersion were also determined for the same set of samples. An additional assessment of sensitivity, specificity, and precision was carried out, and the obtained values corresponding to the two examined methods were compared. The obtained results revealed the advantages and disadvantages of the developed approach to speckle pattern analysis for neurodiagnostics.

Studied samples

Glioblastoma is a rapidly growing, poorly differentiated, and treatment-refractory brain tumor. In its histobiological properties, glioma model 101.8 is close to malignant gliomas of the human brain. A transplantable malignant rat glioma (strain 101.8) model has been obtained for the first time at the Research Institute of Human Morphology [23]. This tumor model is characterized by invasive ingrowth into tissues surrounding the brain, which makes it difficult to define clearly its boundaries with intact tissues.

Rat brain tissue samples were examined *ex vivo*. More detailed data are provided in Table 1. Experiments with laboratory animals were carried out at the Avtsyn Research Institute of Human Morphology (Federal State Budgetary Scientific Institution „Petrovsky National Research Centre of Surgery,"Moscow, Russia) in accordance with the following international ethical standards and principles: (1) European Convention for the Protection of Vertebrate Animals used for Experimental and Other Scientific Purposes (Strasbourg, 2006); (2) International Guiding Principles for Biomedical

Research Involving Animals (Council for International Organizations of Medical Sciences and International Council for Laboratory Animal Science, 2012); and (3) three Rs principle (when possible, laboratory animals in experiments are replaced by alternative models, the number of animals studied is reduced, and the experimental methodology is refined to minimize pain and enhance the welfare of animals). The studies were conducted in accordance with the internal guidelines of the Avtsyn Research Institute of Human Morphology. Only qualified personnel were allowed to work with animals, which ensured compliance with standards and ethical principles. All animals were kept in appropriate conditions, and experimental procedures were performed with account for their condition to ensure reliability of the obtained data.

Twelve mature male Wistar rats with glioma model 101.8 were studied (Table 1). Rat brain tissue samples were dissected into two parts, and the frontal part was subjected to OCT no later than 10 min after resection. An OCT1300Y system developed at the Institute of Applied Physics of the Russian Academy of Sciences in Nizhny Novgorod was used for measurements. A superluminescent diode with an operating wavelength of $1.3\,\mu$m and an optical output power of 0.6 mW served as the optical radiation source. The samples were covered with a gelatin film to prevent hydration and dehydration in the process of measurements. Following measurements, all tissues were fixed in formalin and transported for histological examination to confirm the preliminary diagnosis. Examples of OCT images of rat brain tissue and the corresponding histological image are presented in Fig. 1.

OCT images output from the system are 400×256 pixels in size, which corresponds to a transverse scan range of 1.96 mm (the resolution is $20\,\mu$m) and a depth scan range of ~ 1 mm (the resolution is $24\,\mu$m in air). Pre-processing was performed (see the diagram in Fig. 2) prior to analysis of OCT images. At the first stage of pre-processing, the region corresponding to the signal from the tissue layer was selected. Distortions introduced by the OCT system were then suppressed by removing 15 side pixels and filtering the image with a transfer function [34].

Attenuation coefficient analysis

Biological tissues are optically heterogeneous absorbing media. Light is scattered off various structures inside the cells. The propagation of light in biological tissues is governed by the scattering and absorbing properties of their components. When biological tissues are illuminated by a laser beam, its attenuation in the single scattering approximation may be characterized by the Bouguer−Lambert−Beer law:

$$I(z) = I_0 \exp(-\mu z), \qquad (1)$$

where I_0 is the incident light intensity;

$$\mu = \mu_a + \mu_s \qquad (2)$$
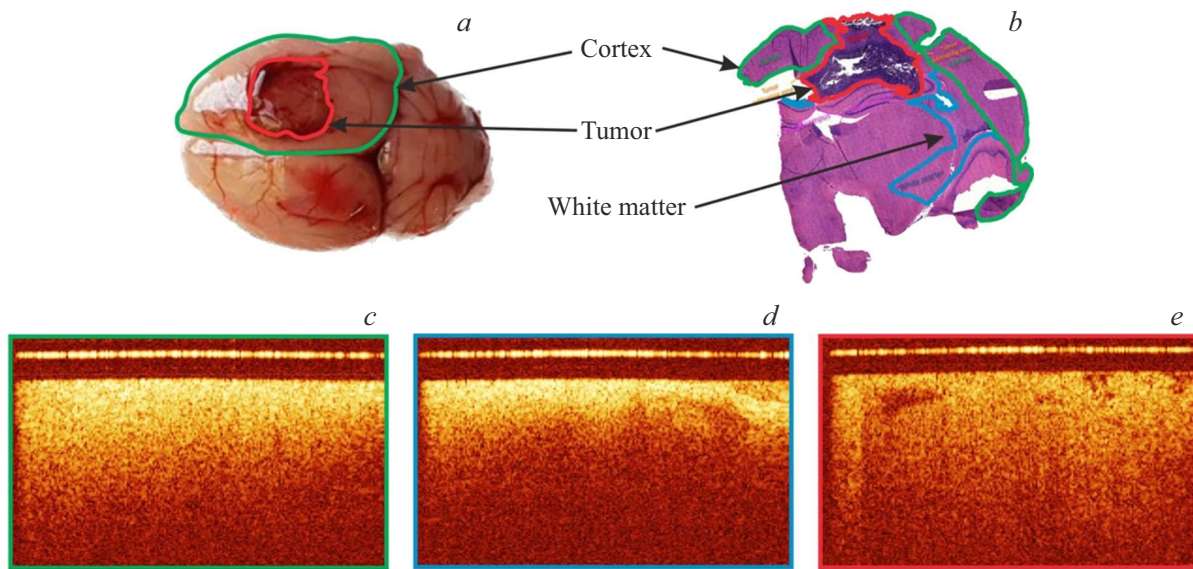
Figure 1. Rat brain images obtained *ex vivo*: (*a*) example of an extracted rat brain; (*b*) histological image of this sample; (*c*–*e*) OCT images of the cortex, white matter, and rat glioma model 101.8, respectively.
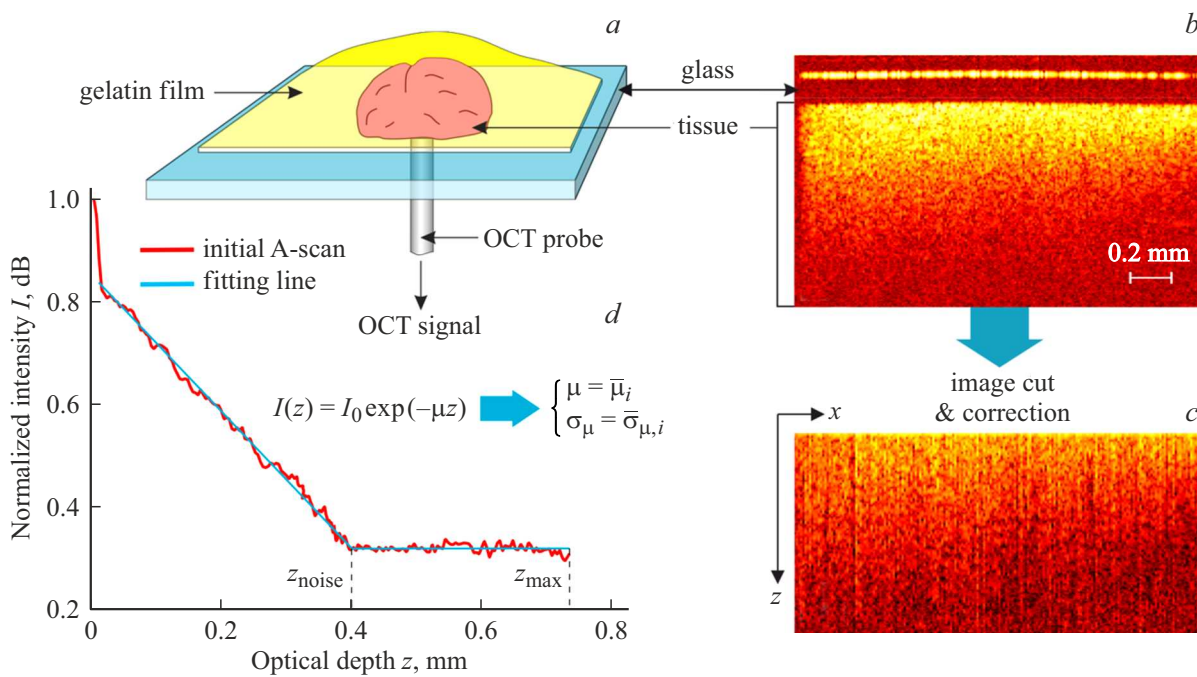
Figure 2. OCT images of a rat brain obtained *ex vivo*: *(a)* diagram of the OCT tissue measurement experiment; *(b)* example initial image obtained prior to cortex processing; *(c)* final image obtained after applying the transfer function and selecting the region corresponding to the tissue of interest; *(d)* extraction of attenuation coefficient μ from a normalized $I(z)$ A-scan.

is the extinction (attenuation) coefficient; and μ_a, μ_s are the absorption and scattering coefficients, respectively. Since radiation scattering off optical inhomogeneities is dominant in most biological tissues, the following approximation is valid: $\mu \simeq \mu_s$.

Attenuation coefficients μ_i for all the corresponding A-scans, where i is the examined A-scan number, were derived from each OCT image. To determine μ_i values

from a single A-scan slope, the noise part of the OCT signal was removed by minimizing the mean square error in polynomial approximation of an A-scan:

$$z_{\text{noise}} = \text{argmin}_z \left[\frac{\Sigma_0^{z_{\text{noise}}}[I(z) - I_{\text{fit}}(z, \mu_i)]^2}{N_{\text{decay}}} \right.$$

$$\left. + \frac{\Sigma_{z=z_{\text{noise}}}^{z_{\text{max}}}[I(z) - I_{\text{noise}}]^2}{N_{\text{noise}}} \right], \qquad (3)$$
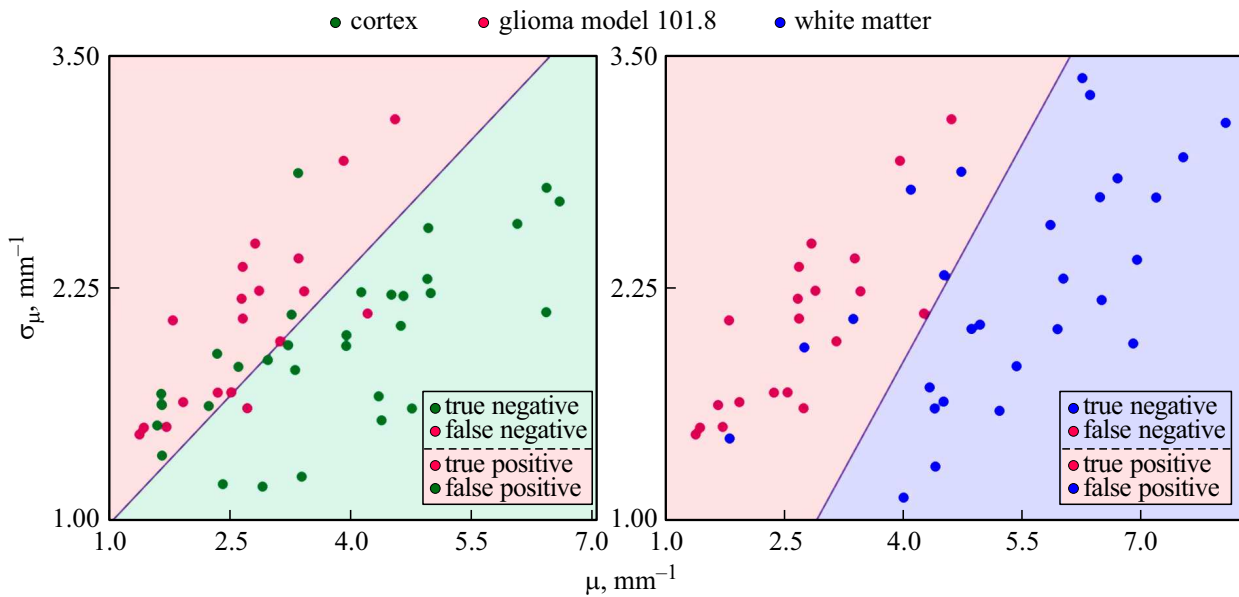
Figure 3. Bivariate distribution of attenuation coefficient μ and standard deviation σ_μ for the considered set of *ex vivo* rat brain tissue samples and separation of classes by LDA.

where $I_{fit}(z, \mu_i)$ is an inclined line; $I_{noise} = I_{fit}(z_{noise}, \mu_i)$ is a horizontal line corresponding to the noise level; z_{max} is the maximum depth of a sample; and N_{decay} and N_{noise} are the numbers of terms in the two corresponding regions of an A-scan. The attenuation coefficient μ analysis reveals the structural properties of tissues, such as their density, cell and nuclei size, and the presence and formation of myelin fibers.

The spread of attenuation coefficient values in OCT images provides information regarding the optical properties of tissue, characterizing its heterogeneity caused by vascularization or necrosis and cysts in glioma tissues. The standard deviation of the attenuation coefficient within a small region in the lateral direction was used as the second parameter:

$$\sigma_{\mu,i} = \left[\sum_{i=1}^{N_A} (\mu_i - \bar{\mu}_i)^2 / N_A \right]^{0.5}, \qquad (4)$$

where $\bar{\mu}_i$ is the local average μ_i value in the region under consideration with its size corresponding to $N_A = 150\,\mu m$ (the typical size of a small vessel in brain tissue). Average values of $\mu = \bar{\mu}_i$ and $\sigma_\mu = \bar{\sigma}_{\mu,i}$ for each OCT image (all its A-scans) were considered in further analysis. These parameters formed the basis for examination of optical properties performed to differentiate glioma from intact tissue.

Bivariate distributions of the discussed parameters are shown in Fig. 3. The attribution of each sample to intact tissues or glioma model 101.8 was verified by histological examination. Different colors of dots in two-dimensional space correspond to different tissue types. The space is divided into two regions using the linear discriminant analysis (LDA) method, which is discussed in more detail below. According to the results for the first method of OCT image analysis (Fig. 4) obtained after LDA and representing the probability of attribution of examined tissues to glioma model 101.8, it is harder to differentiate between the cortex and the glioma model than between white matter and the glioma model, since white matter is characterized by the presence of nerve fibers and, consequently, an enhanced attenuation coefficient.

Wavelet analysis of speckle patterns

Wavelet analysis is often used as a noise filtering method for OCT images [35]. Its efficiency is attributable to the fact that basis functions of the wavelet transform are similar in their properties to wave packets (zero mean value, boundedness, and simultaneous localization in the time and frequency domains). This method also allows one to identify inhomogeneities in images. Lingley−Papadopoulos *et al.* [36] were the first to demonstrate the use of wavelet analysis in combination with texture analysis of OCT images for the detection of cancer tissue. Essock *et al.* [37] have investigated the feasibility of application of wavelet OCT image analysis in glaucoma detection. The wavelet analysis method, which forms the basis of image processing, provides an opportunity to separate the informative part of the signal from noise (speckle noise included), enhancing the signal-to-noise ratio. Thus, wavelet analysis is an efficient instrument for extracting the characteristics of speckle patterns in OCT images.

In the present study, discrete wavelet transform, which allows one to analyze various frequency components, was

Probability of tissue attribution to glioma model 101.8

Attenuation features [μ; σ_μ]
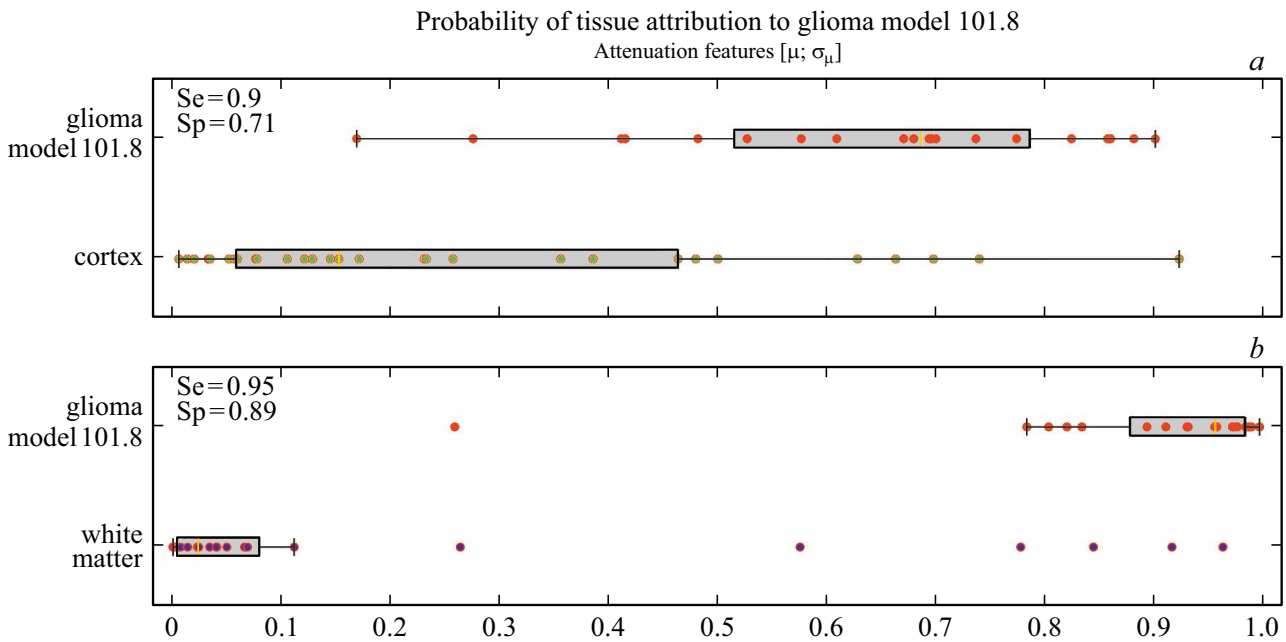
Figure 4. Difference between glioma model 101.8 and intact brain tissues ((*a*) cortex and (*b*) white matter) determined by LDA of optical parameters. Dots are colored according to the results of histological analysis of the considered tissue types. Box-and-whiskers plots represent the quartile values (lower — 25th percentile (Q_1), upper — 75th percentile (Q_3)), the minimum and maximum values in subset $Q_1 \mp 1.5(Q_3 - Q_1)$ — „whiskers," and the median (50th percentile).

used for OCT image processing. The two-dimensional discrete wavelet transform is based on the one-dimensional wavelet transform, which does not depend on the number of columns and lines of images. With the wavelet transform, the signal is decomposed into low-frequency (approximation) and high-frequency (detail) components. The signal is decomposed into levels, each of which produces two sets of detail and approximation coefficients. Detail and approximation coefficients are associated with high-frequency and low-frequency data, respectively. Since our goal is to evaluate the possibility of differentiating between brain tissue and glioma using speckle pattern analysis, only detail coefficients are considered below.

Wavelet filter bior 3.5 (biorthogonal filter) was used for the wavelet transform. The efficiency of bior 3.5 has been demonstrated earlier in [38]. However, it is important to note that the choice of wavelet filter depends on the OCT system used. It has been demonstrated already that only the first and second levels of OCT image decomposition contain data on speckle patterns [39]. An example decomposition of an OCT image into detail coefficients (VDC, HDC, DDC — vertical, horizontal, and diagonal coefficients, respectively) with the bior 3.5 wavelet filter for glioma model 101.8 is presented in Fig. 5.

The power of local brightness fluctuations in a speckle was chosen as the primary parameter of wavelet analysis of

OCT images with regard to speckle patterns:

$$P_a = \frac{1}{K} \left[\left| \sum_{n_x, n_y} I_a^{\mathrm{HDC}}(n_x, n_y) \right|^2 + \left| \sum_{n_x, n_y} I_a^{\mathrm{VDC}}(n_x, n_y) \right|^2 + \left| \sum_{n_x, n_y} I_a^{\mathrm{DDC}}(n_x, n_y) \right|^2 \right], \quad (5)$$

where $K = N_x N_y$ is the number of pixels in an image; n_x, n_y is the current position of the examined pixel; I_a^{HDC}, I_a^{VDC}, and I_a^{DDC} are the intensities of horizontal, vertical, and diagonal detail coefficients, respectively; and a is the image decomposition level.

The standard deviation of the power of local brightness fluctuations in a speckle was the auxiliary parameter:

$$\sigma_{Pa} = \left[\sum_{n_x=1}^{N_x^*} \left(P_a^x(n_x) - P_a \right)^2 / N_x^* \right]^{0.5}. \quad (6)$$

Here, $P_a^x(n_x)$ is the mean power in direction Y for each pixel n_x:

$$P_a^x(n_x) = \frac{1}{N_y} \left[\left| \sum_{n_y} I_a^{\mathrm{HDC}}(n_x, n_y) \right|^2 + \left| \sum_{n_y} I_a^{\mathrm{VDC}}(n_x, n_y) \right|^2 + \left| \sum_{n_y} I_a^{\mathrm{DDC}}(n_x, n_y) \right|^2 \right]. \quad (7)$$
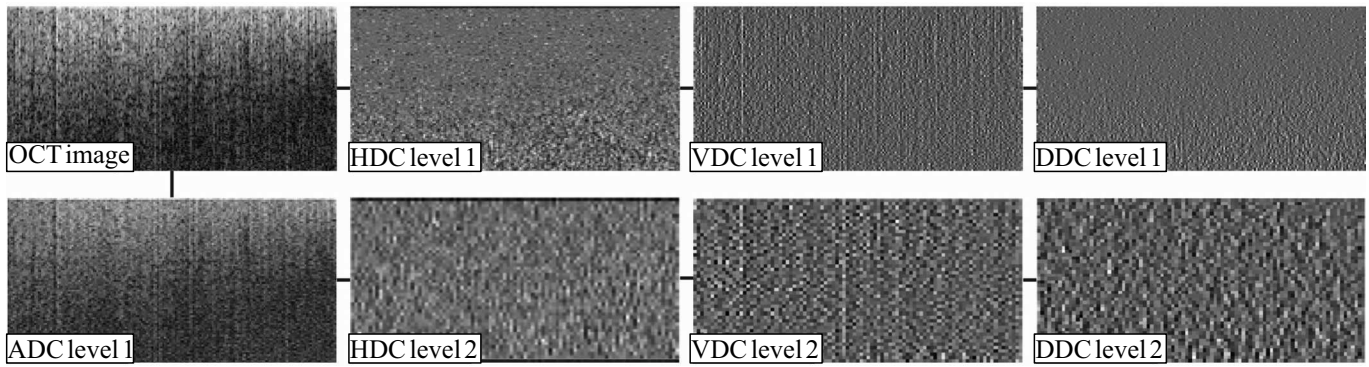
Figure 5. Example decomposition of an OCT image into detail (horizontal HDC, vertical VDC, and diagonal DDC) and approximation (ADC) coefficients at two decomposition levels.
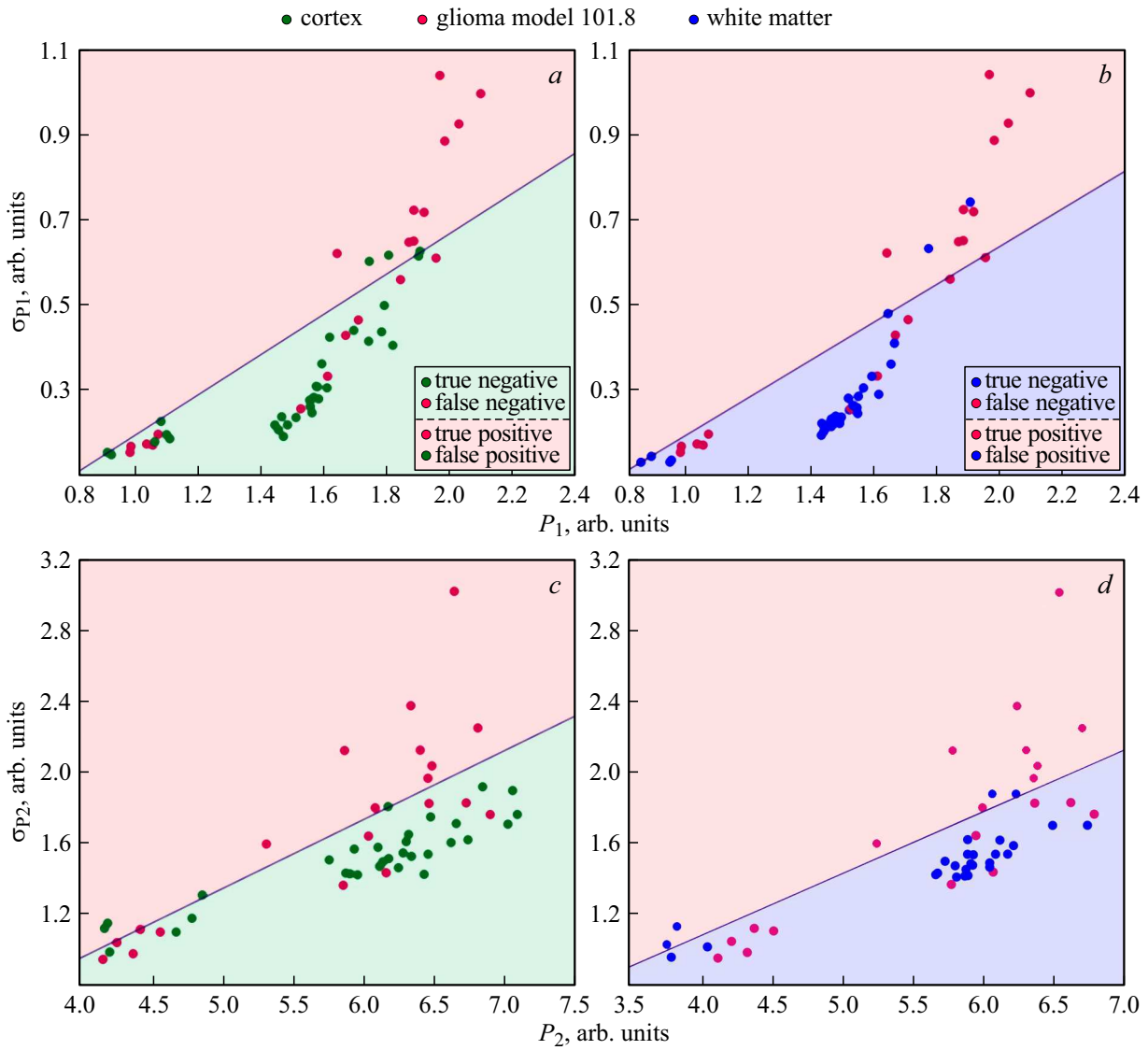
Figure 6. Bivariate distribution of the power of local brightness fluctuations in a speckle at two decomposition levels $P_{1,2}$ and standard deviation $\sigma_{P_{1,2}}$ for the considered set of *ex vivo* rat brain tissue samples and separation of classes with LDA: (a, b) — results for the first level of decomposition; (c, d) — results for the second level.
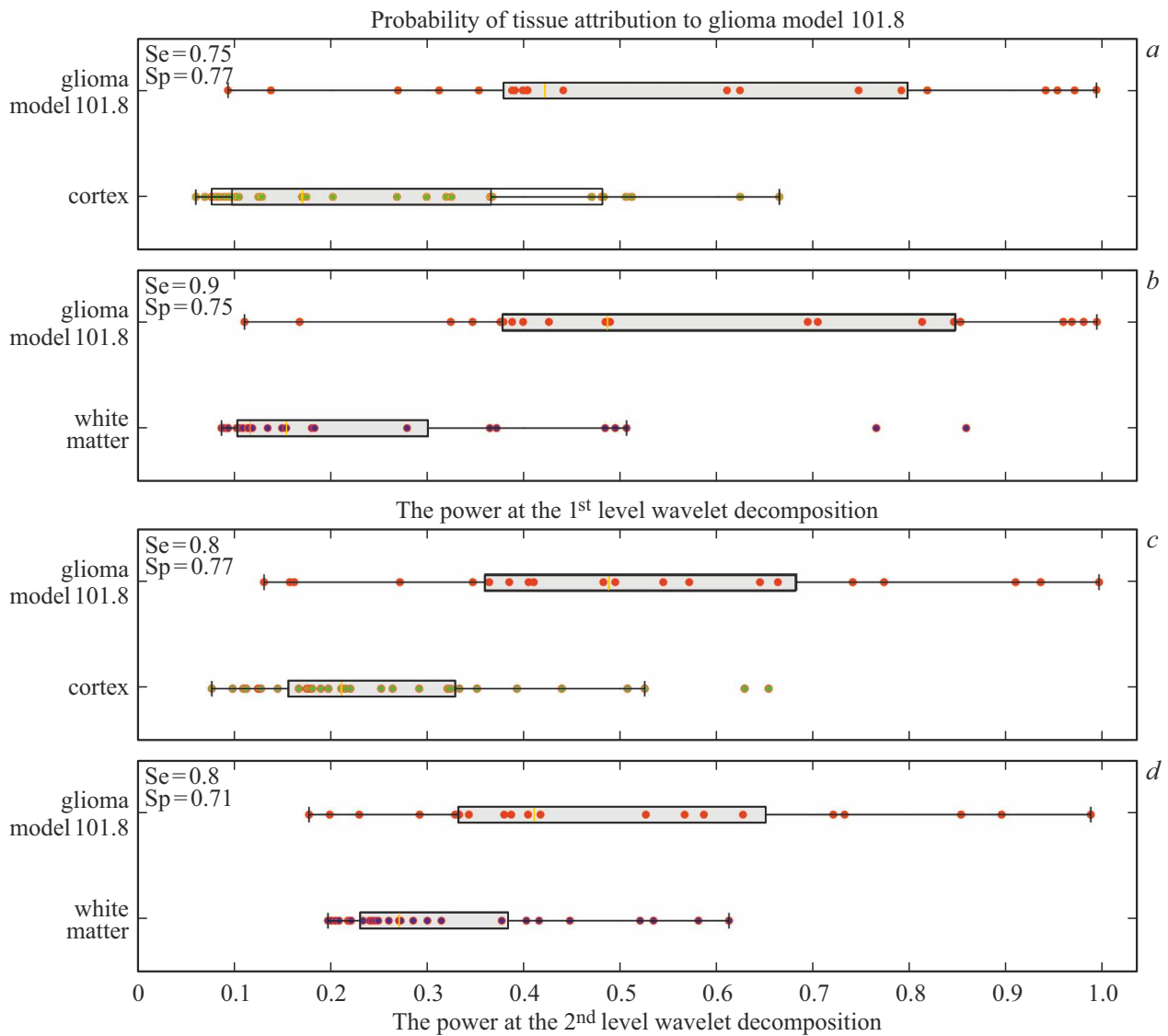
Figure 7. Difference between glioma model 101.8 and intact brain tissues ((a, c) cortex and (b, d) white matter) determined by LDA of the power of local brightness fluctuations in speckles at the first (a, b) and the second (c, d) decomposition levels. Dots are colored according to the results of histological analysis of the considered tissue types. Box-and-whiskers plots represent the quartile values (lower — 25th percentile (Q_1), upper — 75th percentile (Q_3)), the minimum and maximum values in subset $Q_1 \mp 1.5(Q_3 - Q_1)$ — „whiskers," and the median (50th percentile).

Two parameters P_a and σ_{Pa} were obtained by averaging the corresponding values for each obtained distribution. The obtained distribution of values for the two-dimensional analysis is presented in Fig. 6. One may note that intact tissues are separated from glioma model 101.8 both at the first and at the second levels of decomposition. The probability of attribution of all the examined tissue types to glioma is shown in Fig. 7. The obtained values suggest that the first level of decomposition of an OCT image is preferable for analysis of the power of local brightness fluctuations in speckles aimed at differentiating between glioma model 101.8 and white matter, while the second level of decomposition is better suited for analysis of the cortex and glioma.

Fisher's linear discriminant analysis (LDA) was used for brain tissue differentiation. The purpose of the LDA method is to determine the maximum distance between the distributions of two different classes of objects and events. The resulting combination is used as a linear classifier:

— a search is performed for a line onto which points are projected based on the Fisher's criterion;

— a search is performed for a discrimination function perpendicular to the Fisher's one based on logistic regression.

A straight line separating two classes of objects with the maximum possible values of sensitivity (Se) and specificity (Sp) is thus obtained based on the actual diagnosis for each considered tissue sample. Sensitivity, specificity, and

Table 2. Estimation of sensitivity Se, specificity Sp, and precision Pr values for differentiation between glioma model 101.8 and intact rat brain tissues with the use of optical parameters $[\mu, \sigma_\mu]$ and power parameter $[P_{1,2}, \sigma_{P_{1,2}}]$ of local brightness fluctuations in speckles at two levels

Tissue types	$[\mu, \sigma_\mu]$			$[P_1, \sigma_{P_1}]$			$[P_2, \sigma_{P_2}]$		
	Se	Sp	Pr	Se	Sp	Pr	Se	Sp	Pr
Cortex vs glioma 101.8	**0.90**	0.71	0.67	0.75	**0.77**	0.68	0.80	**0.77**	**0.69**
White matter vs glioma 101.8	**0.95**	**0.89**	**0.86**	0.90	0.75	0.72	0.80	0.71	0.67

precision (Pr) parameters were analyzed additionally:

$$\text{Se} = \frac{\text{TP}}{\text{TP+FN}}, \qquad (8)$$

$$\text{Sp} = \frac{\text{TN}}{\text{TN+FP}}, \qquad (9)$$

$$\text{Pr} = \frac{\text{TP}}{\text{TP+FP}}, \qquad (10)$$

where TP is a true positive parameter, TN is a true negative parameter, FP is a false positive parameter, and FN is a false negative parameter.

Analysis of the obtained results

Two methods for analysis of OCT images and their subsequent processing by Fisher's LDA were examined. The values of sensitivity, specificity, and precision were calculated as additional numerical parameters for assessment of tissue differentiation. The obtained values for two processing methods are presented in Table 2.

As can be seen from Table 2, Fisher's LDA confirms that attenuation coefficient μ is the preferable parameter for brain tissue differentiation in the case of white matter and glioma model 101.8. However, the method of wavelet analysis of OCT image speckles allows one to raise the level of specificity and precision in differentiating between the cortex and glioma model 101.8.

Conclusion

The application of two developed methods for OCT image analysis was demonstrated. The first one involves extracting the attenuation coefficient and its dispersion, and the second method is based on the analysis of power and dispersion of local brightness fluctuations in a speckle. Samples of rat brain tissues, which included the cortex, white matter, and glioma model 101.8, were examined *ex vivo*. LDA with subsequent calculation of sensitivity, specificity, and precision levels was used to evaluate the efficiency of the developed methods. The obtained results revealed the advantages of analyzing the optical parameters of OCT images of brain tissues compared to the application of wavelet analysis. However, the power of local brightness fluctuations in a speckle may also be used as an additional parameter to enhance the specificity of diagnosis in differentiating between the cortex and the rat glioma model.

Funding

Conflict of interest

The authors declare that they have no conflict of interest.

References

[1] A. Fercher, K. Mengedoht, W. Werner. Opt. Lett., **13**, 186−188 (1988). DOI: 10.1364/OL.13.000186

[2] C.K. Hitzenberger. Invest Ophthalmol Vis Sci., **32** (3), 616−624 (1991). PMID: 2001935

[3] D. Huang, E.A. Swanson, C.P. Lin, J.S. Schuman, W.G. Stinson, W. Chang, M.R. Hee, T. Flotte, K. Gregory, C.A. Puliafito, D. Huang. Science, **254** (5035), 1178−1181 (1991). DOI: 10.1126/science.1957169

[4] W. Drexler, J. Fujimoto. *Optical Coherence Tomography: Technology and Applications,* 2nd ed. (Springer Reference, 2015).

[5] B.E. Bouma, J.F. de Boer, D. Huang, I.K. Jang, T. Yonetsu, C.L. Leggett, R. Leitgeb, D.D. Sampson, M. Suter, B. Vakoc, M. Villiger, M. Wojtkowski. Nat Rev. Methods Primers, **2** (79), (2022). DOI: 10.1038/s43586-022-00162-2

[6] M.I. Su, C.Y. Chen, H.I. Yeh, K.T. Wang. Acta Cardiol. Sin., **32** (4), 381−386 (2016). DOI: 10.6515/acs20151026a

[7] E. Osiac, T.A. Bălşeanu, B. Cătălin, L. Mogoantä, C. Gheonea, S.N. Dinescu, C.V. Albu, B.V. Cotoi, O.S. Tica, V. Sfredel. Rom. J. Morpho.l Embryol., **55** (2 Suppl), 507−512 (2014). PMID: 25178320

[8] R.K. Murthy, S. Haji, K. Sambhav, S. Grover, K.V. Chalam. Biomed. J., **39** (2), 107−120 (2016). DOI: 10.1016/j.bj.2016.04.003

[9] Y. Zhang, Y. Chen, Y. Yu, X. Xue, V.V. Tuchin, D. Zhu. J. Biomed. Opt., **18** (7), 077003 (2013). DOI: 10.1117/1.JBO.18.7.077003

[10] K.S. Yashin, L.Ya. Kravets N.D. Gladkova, G.V. Gelikonov, I.A. Medyanik, M.M. Karabut, E.B. Kiseleva, P.A. Shilyagin. Burdenko's Journal of Neurosurgery, **3**, 87−94 (2017). DOI: 10.17116/engneiro201781387-94

[11] S.A. Boppart, B.E. Bouma, C. Pitris, G.J. Tearney, J.F. Southern, M.E. Brezinski, J.G. Fujimoto. Radiology, **208** (1), 81−86 (1998). DOI: 10.1148/radiology.208.1.9646796

[12] M.S. Jafri, S. Farhang, R.S. Tang, N. Desai, P.S. Fishman, R.G. Rohwer, C.-M. Tang, J.M. Schmitt. J. Biomed. Opt., **10** (5), 051603 (2005). DOI: 10.1117/1.2116967

[13] S.W. Jeon, M.A. Shure, K.B. Baker, D. Huang, A.M. Rollins, A. Chahlavi, A.R. Rezai. J. Neurosci. Methods., **154** (1−2), 96−101 (2006). DOI: 10.1016/j.jneumeth.2005.12.008

[14] H.J. Böhringer, D. Boller, J. Leppert, U. Knopp, E. Lankenau, E. Reusche, G. Hüttmann, A. Giese. Lasers Surg. Med., **38** (6), 588−597 (2006). DOI: 10.1002/lsm.20353

[15] H.J. Böhringer, E. Lankenau, F. Stellmacher, E. Reusche, G. Hüttmann, A. Giese. Acta Neurochir. (Wien), **151** (5), 507−517 (2009). DOI: 10.1007/s00701-009-0248-y

[16] W.O. Contreras Lopez, J.S. Ângelos, R.C.R. Martinez, C.K. Takimura, M.J. Teixeira, P.A. Lemos Neto, E.T. Fonoff. Braz. J. Med. Biol. Res., **48** (12), 1156−1159 (2015). DOI: 10.1590/1414-431X20154679

[17] C. Kut, K.L. Chaichana, J. Xi, S.M. Raza, X. Ye, E.R. McVeigh, F.J. Rodriguez, A. Quiñones-Hinojosa, X. Li. Sci. Transl. Med., **7** (292), 292ra100 (2015). DOI: 10.1126/scitranslmed.3010611

[18] K.S. Yashin, E.B. Kiseleva, E.V. Gubarkova, A.A. Moiseev, S.S. Kuznetsov, P.A. Shilyagin, G.V. Gelikonov, I.A. Medyanik, L.Y. Kravets, A.A. Potapov, E.V. Zagaynova, N.D. Gladkova. Front. Oncol., **9**, 201 (2019). DOI: 10.3389/fonc.2019.00201

[19] K.S. Yashin, E.B. Kiseleva, A.A. Moiseev, S.S. Kuznetsov, L.B. Timofeeva, N.P. Pavlova, G.V. Gelikonov, I.A. Medyanik, L.Y. Kravets, E.V. Zagaynova, N.D. Gladkova. Sci. Rep., **9** (1), 2024 (2019). DOI: 10.1038/s41598-019-38493-y

[20] I.N. Dolganova, P.V. Aleksandrova, P.V. Nikitin, A.I. Alekseeva, N.V. Chernomyrdin, G.R. Musina, S.T. Beshplav, I.V. Reshetov, A.A. Potapov, V.N. Kurlov, V.V. Tuchin, K.I. Zaytsev. Biomed. Opt. Express, **11** (11), 6780−6798 (2019). DOI: 10.1364/BOE.409692

[21] S.J. Madsen. *Optical methods and instrumentation in brain imaging and therapy,* 1st ed. (Springer, 2013), 3. DOI: 10.1007/978-1-4614-4978-2

[22] S.C.J. Steiniger, J. Kreuter, A.S. Khalansky, I.N. Skidan, A.I. Bobruskin, Z.S. Smirnova, S.E. Severin, R. Uhl, M. Kock, K.D. Geiger, S.E. Gelperina. Int. J. Cancer, **109** (5), 759−67 (2004). DOI: 10.1002/ijc.20048

[23] V.V. Fedoseeva, E.A. Postovalova, A.S. Khalansky, V.A. Razzhivina, S.E. Gelperina, O.V. Makarova. Sovremennye Technologii v Medicine, **10** (4), 105−112 (2018). DOI: 10.17691/stm2018.10.4.12

[24] N.D. Gladkova, K.A. Achkasova, K.S. Yashin, E.B. Kiseleva, A.A. Moiseev, E.L. Bederina, S.S. Kuznetsov, I.A. Medyanik, L.Ya. Kravets, G.V. Gelikonov, P.A. Shilyagin. *Optical Coherence Tomography in Brain Gliomas Detection and Peritumoral White Matter State Evaluation,* 1st ed. (Springer, Singapore, 2022), p. 1−22. DOI: 10.1007/978-981-19-1352-5_1

[25] H.J. Böhringer, D. Boller, J. Leppert, U. Knopp, E. Lankenau, E. Reusche, G. Hüttmann, A. Giese. Lasers Surg. Med., **38** (6), 588−597 (2006). DOI: 10.1002/lsm.20353

[26] C. Kut, K.L. Chaichana, J. Xi, S.M. Raza, X. Ye, E.R. McVeigh, F.J. Rodriguez, A. Quiñones-Hinojosa, X. Li. Science Translational Medicine, **7** (292), 292ra100 (2015). DOI: 10.1126/scitranslmed.3010611

[27] K. Bizheva, A. Unterhuber, B. Hermann, B. Povazay, H. Sattmann, A.F. Fercher, W. Drexler, M. Preusser, H. Budka, A. Stingl, T. Le. J. Biomed. Opt., **10** (1), 11006 (2005). DOI: 10.1117/1.1851513

[28] N. Mazumber, G. Gangadharan, Y.V. Kistenev. *Advances in Brain Imaging Techniques,* 1st ed. (Springer, Singapore, 2022). DOI: 10.1007/978-981-19-1352-5

[29] J.M. Schmitt, S.H. Xiang, K.M. Yung. J. Biomed. Opt., **4** (1), 95−105 (1999). DOI: 10.1117/1.429925

[30] M. Almasian, T.G. van Leeuwen, D.J. Faber. Sci. Rep., **7** (1), 14873 (2017). DOI: 10.1038/s41598-017-14115-3

[31] M. Cua, B. Blochet, C. Yang. Biomed. Opt. Express, **13** (4), 2068−2081 (2022). DOI: 10.1364/BOE.448969

[32] A. Mcheik, C. Tauber, H. Batatia, J. George, J.-M. Lagarde. In: Conference: VISAPP 2008, ed. by A. Ranchordas, H. Araújo. *Proceedings of the Third International Conference on Computer Vision Theory and Applications* (Funchal, Madeira, Portugal, 2008), vol. 1, pp. 347−350.

[33] D.A. Jesus, D.R. Iskander. Biomed. Opt. Express, **8** (1), 162−176 (2017). DOI: 10.1364/BOE.8.000162

[34] H. Wang, C. Magnain, S. Sakadžić, B. Fischl, D.A. Boas. Biomed. Opt. Express, **8** (12), 5617−5636 (2017). DOI: 10.1364/BOE.8.005617

[35] J.-L. Strack, A. Bijaoui. Signal Process, **35** (3), 195−211 (1994). DOI: 10.1016/0165-1684(94)902011-9

[36] C.A. Lingley-Papadopoulos, M.H. Loew, J.M. Zara. J. Biomed. Opt., **14** (4), 044010 (2009). DOI: 10.1117/1.3171943

[37] E.A. Essock, Y. Zheng, P. Gunvant. Invest. Ophthalmol. Vis. Sci., **46** (8), 2838−2847 (2005). DOI: 10.1167/iovs.04-1156

[38] I.N. Dolganova, N.V. Chernomyrdin, P.V. Aleksandrova, S.T. Beshplav, A.A. Potapov, I.V. Reshetov, V.N. Kurlov, V.V. Tuchin, K.I. Zaytsev. J. Biomed. Opt., **23** (9), 1−9 (2018). DOI: 10.1117/1.JBO.23.9.091406

[39] C. Buranachai, P. Thavarungkul, P. Kanatharanaa, I.V. Meglinski. Laser Phys. Lett., **6** (12), 892−895 (2009). DOI: 10.1002/lapl.200910089

Translated by D.Safin